

Quantum Circuits Noise Tailoring from a Geometric Perspective

Junkai Zeng,^{1,2} Yong-Ju Hai,² Hao Liang,^{1,2} and Xiu-Hao Deng^{1,2,*}

¹*Shenzhen Institute for Quantum Science and Engineering (SIQSE),
Southern University of Science and Technology, Shenzhen, P. R. China*

²*International Quantum Academy (SIQA), and Shenzhen Branch,
Hefei National Laboratory, Fudan District, Shenzhen, P. R. China*

(Dated: May 12, 2023)

Quantum errors subject to noisy environments remain a major obstacle to advancing quantum information technology. Solutions to this issue include robust quantum control at the pulse level and error correction or mitigation techniques at the circuit level. We develop a geometric method to unify the treatments of noises at both levels to understand noisy dynamics and reduce errors. We illustrate the error's random walk in the geometric space to explain how coherent noises are tailored into stochastic Pauli errors by randomized compiling. We obtain analytical formulas for the noise parameters and show how robust quantum control techniques can further improve circuit fidelity. We demonstrate the efficacy of our approach using numerical simulations, showcasing its potential for advancing quantum information processing.

Introduction.-Quantum computing can tackle complex problems beyond classical computing[1–3], but noises from sources like environmental coupling and control errors can impair quantum circuits. Researchers have devised various techniques to combat these noises. Robust quantum control designs and implements control pulses that minimize noise and other perturbations on the quantum system [4–14]. By engineering pulse sequences, robust control allows for the precise manipulation of quantum states in the presence of noise and hence becomes an essential tool for enhancing the performance of quantum computing systems [15–22]. Nonetheless, it is important to recognize that quantum circuits can also resist noise inherently without relying on robust gates. Randomized compiling (RC) has been proposed as an alternative technique that mitigates noise at the circuit level [23–26]. It applies random operations, called twirling gates, to transform a given quantum circuit into equivalent circuits. By averaging over multiple equivalent circuits, the coherent noise in the system is converted into stochastic, Pauli-like noise. This technique has demonstrated significant improvements in quantum circuit fidelity.

Recently, a novel geometric approach to robust quantum control has been developed known as the Space Curve Quantum Control (SCQC) formalism [27–33]. This theory utilizes geometric curves in a space spanned by affected operators to represent and analyze the quantum error accumulation by various noises. It enables access to explore all possible noise-resistant control Hamiltonians to implement universal robust quantum gates [32]. In this manuscript, we discover that this geometric perspective could be generalized from the pulse level to the circuit level to analyze how gate sequences impact quantum error accumulation. We introduce a general geometric framework that represents quantum errors as curves in an N -dimensional space, where $N = 4^m - 1$ and m is the number of qubits. In this framework, the RC process could now be illustrated as the error curves

going in a random walk process by the random twirling gates, providing a geometric illustration of error propagation and the effectiveness of RC in mitigating errors due to coherent noises. We then show that tomographic analysis of the error subject to different noise channels could proceed by calculating the Pauli transfer matrix (PTM), which makes it possible to combine error mitigation techniques with classical computing resources to further improve quantum circuit fidelity [34, 35]. This general framework further allows the integration of robust quantum control techniques to the gate sequences, resulting in significant improvement of quantum circuit fidelity. Therefore, our theory offers a deeper understanding of the nature and propagation of quantum errors, and opens up possibilities for the development of more effective error correction schemes.

Geometric Formalism.- We introduce the geometric formalism by first exploring generic quantum dynamics and then extending our analysis to quantum circuit models. We consider a multi-qubit system subject to coherent noise, represented as a term in the qubit system Hamiltonian. The system Hamiltonian is expressed as: $H(t) = H_0(t) + \sum_i \epsilon_i(t) \delta H_i$. Here, H_0 denotes the noise-free part of the Hamiltonian, while δH_i represents the noise with a corresponding strength, $\epsilon_i(t)$. The time dependency of the noise can take various forms, such as constant, randomly fluctuating, drifting at a particular speed, or proportional to control amplitude, depending on the noise source. For coherent noise, the form is typically a Pauli matrix in the case of a single-qubit system or the tensor products of Pauli matrices for multi-qubit systems.

The evolution operator associated with the noise effect can be decomposed into two parts:

$$U(t) = U_0(t)U_\epsilon(t) \quad (1)$$

Here the primary unitary $U_0(t)$ corresponds to the noise-free Hamiltonian $H_0(t)$, and the error unitary oper-

ator $U_\epsilon(t)$ corresponds to the noise Hamiltonian in the so-called toggling frame, a frame that rotates with $U_0(t)$. As the noise ϵ is generally small, we can use Magnus expansion and obtain: $U_\epsilon(t) = e^{-i\Phi(t) - \frac{1}{2} \int_0^t [\hat{\Phi}(s), \Phi(s)] ds} + \mathcal{O}(\epsilon^3)$, with the error phase operator Φ given by

$$\Phi(t) = \int_0^t \sum_i \epsilon_i(s) U_0^\dagger(s) \delta H_i U_0(s) ds \quad (2)$$

Following the geometric approach introduced in [33], we decompose the error phase operator and obtain:

$$\Phi(t) = \sum_{ij} \hat{\sigma}_j \int_0^t \epsilon_i(s) r'_{i,j}(s) ds \equiv \sum_{ij} \hat{\sigma}_j R_j^{\epsilon(i)}(t) \quad (3)$$

Here, $\hat{\sigma}_j$ is the j -th generalized Pauli matrix, and for continuous quantum dynamics, $r_{i,j}(t)$ traces a smooth curve in an Euclidean space spanned by operators affected by the noise, and the j -th component of the curve measures the amount of error caused by the i -th noise source at evolution time t , and the constraint $\sum_j d(r_{i,j})^2 = dt^2$ must be satisfied for the curve. In the following context we refer to such space as *error geometric space*. For continuous qubit dynamics, the time-dependent Hamiltonian can be reconstructed from the general curvature of the space curve. The simplest example is the resonantly-driven single qubit coupled to quasi-static dephasing noise, where the driving field amplitude correspond to the curvature of a curve lying in a two dimensional plane.

Instead of continuous quantum dynamic, in this paper we focus on the geometric formalism for quantum circuits. To simplify the discussion, we will omit the noise source index i and use the symbol $R_j = \sum_i R_j^{\epsilon(i)}$.

For a generic multi-qubit gate, or a layer in a quantum circuit, Eq. 1 can be interpreted as a target gate U_0 preceded by a error operator $U_\epsilon = e^{-i\hat{\Phi}}$. We still have $\hat{\Phi} = \mathbf{R} \cdot \hat{\sigma}$, and the vector \mathbf{R} represents a vector in the error geometric space. We can move the error operator around in the circuit to analyze the effect of noise on the circuit. Specifically, we have $e^{-i\hat{\Phi}} \hat{C} = \hat{C} e^{-i\hat{C}^\dagger \hat{\Phi} \hat{C}}$, where \hat{C} is a unitary operator representing a chunk of the quantum circuit formed by one or more circuit layers. To observe how the noise effect accumulates as the circuit runs, we can move all error operators to the beginning of the circuit, so that we have:

$$\hat{\Phi}_{\text{total}} = \sum_{ij} R_j^{\epsilon(i)} \hat{\sigma}_j = \sum_i \mathbf{R}^{(i)} \cdot \hat{\sigma} \quad (4)$$

Here i is summed over the number of layers in the circuit, N_D , and j covers all indices of the generalized Pauli matrices. The vector component $R_j^{\epsilon(i)} = \frac{1}{D} \text{Tr}(\hat{C}^{(i)\dagger} (\mathbf{R}_{\text{lo}}^{(i)} \cdot \hat{\sigma}) \hat{C}^{(i)} \hat{\sigma}_j)$, where $\mathbf{R}_{\text{lo}}^{(i)}$ is the local error step at circuit layer i , and $\hat{C}^{(i)}$ represents the circuit

from the beginning to i 'th layer. Since $\hat{C}^{(i)}$ is unitary and thus norm-preserving, error vectors $\mathbf{R}^{(i)}$ and $\mathbf{R}_{\text{lo}}^{(i)}$ are connected through a coordinate transformation. Therefore, Eq. 4 represents a path formed by N_D steps in the error geometric space, with each step vector being $\mathbf{R}^{(i)}$.

Noise Tailoring With Twirling Gates.- We now introduce twirling gates and the noise tailoring technique. The concept of noise tailoring involves adding random gates to eliminate the coherence of the noise while preserving the incoherent contribution. We assume that these random gates are easy to implement and do not introduce additional errors to the circuit, which is a reasonable assumption as twirling gates are mostly chosen from single qubit Clifford gates. Here we derive how quantum circuits can benefit from this technique using the geometric picture.

We consider a twirling operator T preceding a gate at a single layer with local noise, represented as $U = U_0 e^{-i(\mathbf{R}_{\text{lo}} \cdot \hat{\sigma})}$. The gate is subsequently followed by a correction operator $T^c = U_0 T^\dagger U_0^\dagger$ to undo the twirling effect. In this context, U is commonly referred to as “hard gates” or “hard layers” due to their noisiness. There are also “easy layers” typically composed of single qubit gates that can be implemented without introducing additional noise. The twirling gate and correction operators are combined with easy gates in the actual gate implementation so that the strategy ensures that the inclusion of twirling gates does not increase the overhead of the quantum circuit with respect to both circuit depth and noise.

We can move the error operator outside the twirling operator and consequently obtain a dressed error operator, that is, $T^c U_0 e^{-i(\mathbf{R}_{\text{lo}} \cdot \hat{\sigma})} T = U_0 e^{-iT^\dagger(\mathbf{R}_{\text{lo}} \cdot \hat{\sigma})T}$. From a geometric perspective, the twirling gate effectively rotates the local error step vector. Specifically, when the twirling operator is selected from the Pauli matrices set, the j -th component of R_{lo} could obtain a minus sign if T and $\hat{\sigma}_j$ do not commute. If all Pauli matrices, including the identity, have an equal chance of being chosen for T , a minus sign may appear at all components of $\hat{\sigma}_j$ with a 50/50 chance, resulting in a symmetrically distributed \tilde{R}_{lo} along all axes. It is important to note that the twirling gate T need not be sampled from the entire Pauli gate set; a smaller set is sufficient when the error does not span the entire Pauli space, as demonstrated in [36].

Focusing on the local error vector step, it is equivalent to a step in a symmetrical random walk process where, at dimension k , it may move forward or backward for a distance of $R_{\text{lo},k}$. In a quantum circuit with multiple layers, $\mathbf{R}_{\text{lo}}^{(i)}$ and $\hat{C}^{(i)}$ are generally different for each i . We can obtain an upper bound using $R_m = \max_i |R_{\text{lo}}^{(i)}|$ so that for each step, we always have $-R_m \leq \tilde{R}_j^{(i)} \leq R_m$, making it a symmetrical one-dimensional random walk process along each axis. Due to the random walk properties, the error distance scales with the circuit depth

as $\sqrt{N_{\text{depth}}}$. It is also worth noting that when the circuit consists of Clifford gates and has the same $\mathbf{R}_{\text{lo}}^{(i)}$ for all i 's, the process reduces to a random walk process in an N-D lattice.

The above analysis focuses on the evolution operator associated with only one run of a quantum circuit, which corresponds to a single trajectory of the error geometric space. To better understand the process when running the circuit multiple times with different twirling gates and averaging the results, as done in experiments, it is helpful to express the process as a quantum noise channel. We write the noise channel for a single layer of the circuit as a mapping of operators, $\mathcal{E}(\hat{P}) = U_\epsilon \hat{P} U_\epsilon^\dagger$. In the following context, we will focus on cases when \hat{P} is a generalized Pauli matrix. The error operator can be expressed in a perturbative way as:

$$U_\epsilon = \exp \left(-i \sum_{n=1}^{\infty} \frac{1}{n!} \sum_i R_i^{[n]} \hat{\sigma}_i \right) \quad (5)$$

Here, $R_i^{[n]}$ represents the amount of n -th order error that appears in the i -axis in Pauli space, which can be calculated with Magnus expansion as shown in [33]. When the error is small, we can write the noise channel as:

$$\begin{aligned} \mathcal{E}(\hat{P}) &= \hat{P} \exp \left(-i \sum_{n=1}^{\infty} \frac{1}{n!} \sum_i R_i^{[n]} \left(\hat{P} \hat{\sigma}_i \hat{P} - \hat{\sigma}_i \right) \right) \\ &= \hat{P} \exp \left(2i \sum_{n=1}^{\infty} \frac{1}{n!} \sum_i R_i^{[n]} \hat{\sigma}_i \right) \end{aligned} \quad (6)$$

The summation over i encompasses all instances where $\hat{\sigma}_i$ and \hat{P} anticommute. It is more insightful to expand the entire channel perturbatively about the noise strength ϵ . To do so, we replace n -th order error by doing $R_i^{[n]} \rightarrow \epsilon^n R_i^{[n]}$ and perform a Taylor expansion on $\mathcal{E}(\hat{P})$ by ϵ . The analytical expression for general n -th order term in the expansion is complicated, but we can briefly discuss the property of these terms. Each term will contain a Pauli product chain with various length, $\mathcal{P}_{i_1, i_2, \dots, i_k} = \hat{\sigma}_{i_1} \hat{\sigma}_{i_2} \dots \hat{\sigma}_{i_k}$ with coefficient $\mathcal{K}_{i_1, i_2, \dots, i_k}$, and summation over all indices i_1, i_2, \dots, i_k is performed. Notice the symmetrical feature of each index i in Eq. 5, \mathcal{K} shall have a permutation symmetry in its index, meaning the value remains constant after changing the order of i_j , and as a result, the summation of $\mathcal{K}_{i_1, i_2, \dots, i_k} \mathcal{P}_{i_1, i_2, \dots, i_k}$ can be reduced to cases where \mathcal{P} exhibits the same symmetry, as all other terms will vanish. This requires $[\hat{\sigma}_{i_{j_1}}, \hat{\sigma}_{i_{j_2}}] = 0$ for all pairs of indices (i_{j_1}, i_{j_2}) in \mathcal{P} .

When applying a random twirling gate T , a Pauli product chain becomes $T^\dagger \hat{\sigma}_{i_1} \hat{\sigma}_{i_2} \dots \hat{\sigma}_{i_n} T$. For a Pauli matrix, it always holds that $T^\dagger \hat{\sigma}_{i_j} T = \pm \hat{\sigma}_{i_j}$, with the plus or minus sign depending on whether the operator commutes with T or not, which occurs half the time. Thus, after averaging multiple shots with randomly chosen twirling gates, we obtain $\mathbb{E}_T (T^\dagger \hat{\sigma}_{i_j} T) = 0$ for $\hat{\sigma}_{i_j} \neq \mathcal{I}$.

Consequently, for most of the index configurations of \mathcal{P} , we get a zero after performing the average, except for cases where the Pauli product chain forms an identity operator. The noise channel in Eq. 6 then transforms from a coherent noise channel to a Pauli channel, as we have $\mathcal{E}(\hat{P}) \propto \hat{P}$. The constraints on the Pauli product chain also affect the number of k . Note that we always have $[\hat{\sigma}_{i_1} \hat{\sigma}_{i_2} \dots \hat{\sigma}_{i_{k-1}}, \hat{P}] = 0$ for odd k , and $\hat{\sigma}_{i_k} = \pm \hat{\sigma}_{i_1} \hat{\sigma}_{i_2} \dots \hat{\sigma}_{i_{k-1}}$ must be satisfied for the entire product chain to equal the identity. This conflicts with the requirement that $\hat{\sigma}_{i_k}$ shall anticommute with \hat{P} , and therefore k must be even.

Based on the above discussion, we can compute the first few terms of the noise channel as an expansion in terms of the noise strength:

$$\begin{aligned} \mathcal{E}_\epsilon^{[0-3]}(\hat{P}) &= \hat{P} - 2 \sum_{\{\hat{\sigma}_i, \hat{P}\}=0} R_i^{[1]} (R_i^{[1]} + R_i^{[2]}) \hat{P} \\ \mathcal{E}_\epsilon^{[4]}(\hat{P}) &= \sum_{\{\hat{\sigma}_i, \hat{P}\}=0} \left(\frac{2R_i^{[1]} \left((R_i^{[1]})^3 - R_i^{[3]} \right)}{3} - \frac{(R_i^{[2]})^2}{2} \right) \hat{P} \\ &+ \sum_{\substack{\{\hat{\sigma}_i, \hat{P}\}=0 \\ [\hat{\sigma}_i, \hat{\sigma}_j]=0 \\ i \neq j}} 2 (R_i^{[1]} R_j^{[1]})^2 \hat{P} \end{aligned} \quad (7)$$

The objective of robust quantum control is to minimize, or eliminate, $R_i^{[j]}$ when implementing a gate, therefore when randomized compiling already contributes to improving circuit robustness, incorporating robust quantum control techniques can further enhance the circuit's resilience, as it shows that even first-order error-resistant quantum gates with $R_i^{[1]} = 0$ can significantly reduce numerous terms in the noise channel.

In our previous discussion, we do not take the inner structure of the noise model into consideration for simplification. However, we can examine it more closely to obtain detailed information on the parameters of the noise channel. We can rewrite $R_j^{[1]} = \sum_i R_j^{\epsilon(i)}(T) = \sum_i \int_0^T \epsilon_i(t) r'_{i,j}(t) dt$, as shown in Eq. 3, and consequently the second-order term in the noise channel can be expressed as follows:

$$\begin{aligned} \langle R_j^{\epsilon(i)}(t) \rangle &= \int_0^t \bar{\epsilon}_i(s) r'_{i,j}(s) ds \\ \langle (R_j^{[1]})^2 \rangle &= \sum_{ik} \langle R_j^{\epsilon(i)}(T) \rangle \langle R_j^{\epsilon(k)}(T) \rangle \\ &+ \sum_{ik} \int_{-\infty}^{\infty} S_{ik}(\omega) F_{ij}^{(1)*}(\omega, T) F_{kj}^{(1)}(\omega, T) d\omega \end{aligned} \quad (8)$$

here the 1st-order *fundamental filter function* is defined as $F_{ij}^{(1)}(\omega, t) = \int_0^t C_\epsilon^{(i)}(s) r'_{i,j}(s) e^{i\omega s} ds$ and $C_\epsilon^{(i)}$ is a time-

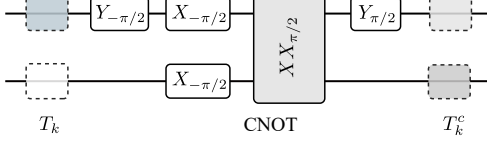


FIG. 1. A visualization of the CNOT circuit. The circuit is composed with an $XX(\pi/2)$ gate and several single qubit Clifford gates. Random twirling gates T_k and the corresponding compensate gates T_k^c are represented with dotted line boxes.

dependent factor that accounts for changes in noise amplitude over time. For example, in the case of multiplicative amplitude noise, we have $C_\epsilon(t) = \Omega(t)$, and $\epsilon_\Omega(t) = \tilde{\epsilon}(t)\Omega(t)$ where $\tilde{\epsilon}(t)$ is a stationary stochastic process. The power spectral density (PSD) $S_{ik}(\omega) = \frac{1}{2\pi} \int_{-\infty}^{\infty} ds e^{-i\omega s} \langle \tilde{\epsilon}_i(s) \tilde{\epsilon}_k(0) \rangle$. Notice that unlike most similar works, we do not assume that the noise is stationary with a zero mean. Although the same approach can be applied to higher-order terms, their expressions can become more complex, so we will not discuss them here.

The discussion in this section makes it possible to derive the parameters of the Pauli noise channel analytically, and this method paves the way for integrating quantum error mitigation techniques with classical resources, ultimately leading to even greater improvements in fidelity.

In summary, randomized compiling can improve circuit fidelity in two ways: 1) For a single quantum circuit, adding random twirling gates transforms the accumulated error curve from a deterministic path to a random walk process; and 2) after averaging multiple shots of many equivalent circuits, the noise channel becomes a Pauli channel as all coherent error terms in the noise channel are eliminated.

Numerical Results.—We consider two specific and simple circuits for demonstration purposes: CNOT and iSWAP. The CNOT circuit consists of a two-qubit gate $XX(\pi/2)$ and several single-qubit gates, as shown in Fig. 1. We assume these single-qubit gates to be noiseless, with the Hamiltonian generating the XX gate given by $\frac{1}{2}\Omega(t)XX$ and noise manifests in the form of $\delta(I\bar{Z} - Z\bar{I} + 0.5ZZ)$. The iSWAP gate is generated by the Hamiltonian $g(XX + YY)$, and a Heisenberg-style $\delta g(XX + YY + ZZ)$ noise term is in presence. For the CNOT circuit, since XX does not commute with either ZI or $I\bar{Z}$, the Hamiltonian for the XX gate can potentially correct errors caused by these noise sources dynamically, while the ZZ term remains unaltered. However, for the iSWAP case, the noise is completely uncorrectable since the noise operator commutes with all terms in the Hamiltonian. These uncorrectable part of the noise makes randomized compiling an essential tool to improve the circuit on top of robust control techniques.

These uncorrectable errors that appear in two-qubit

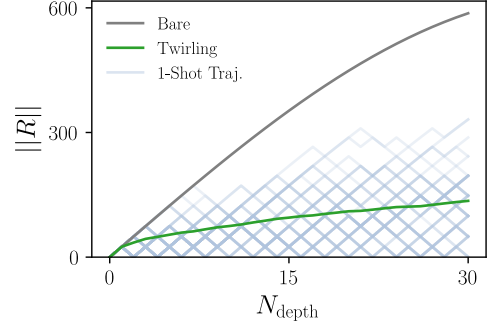


FIG. 2. Error distances of the iSWAP circuit as the circuit depth grows for the cases of the bare circuit, the single-shot trajectory of randomly-applied twirling gates, and the averaged randomized compiled circuits.

gates will accumulate as the circuit goes deeper. We quantify the error accumulated in the circuit through the error distance $\|\mathbf{R}\|$, and we can see that for the iSWAP case, the error distance forms a straight line as the circuit goes deeper. Such a situation corresponds to a worst-case scenario, for which the randomized compiling technique can significantly improve fidelity.

In Fig. 2, we show that the error distance behaves in a one-dimensional random walk pattern as the circuit grows, so the error accumulates tremendously slower than the raw iSWAP circuit. We also show that with multiple instances with differently sampled twirling gates, the average error distance grows as the square root of the depth of the circuit, as the property of a random walk process.

The advantages of implementing twirling gates are not limited to situations where the circuit is deep. We now focus on a single circuit layer to observe fidelity improvements from randomized compiled circuits, which are averaged over multiple equivalent circuits with different twirling gate configurations. The state transfer fidelity under different noise strength, both with and without twirling gates, is compared in Fig. 3. The inclusion of random twirling gates leads to a significant enhancement of fidelity, a trend clearly illustrated in the figure for both CNOT and iSWAP circuits.

Because part of the noise source in the CNOT circuit is potentially correctable, we also incorporated optimal quantum control techniques so that several components in $\mathbf{R}^{[1]}$ vanish. The corresponding $\pi/2$ pulses with an optimized shape obtained in [32] and a trivial cosine shape are shown in Fig. 4. The optimal control pulse exhibit robustness against $I\bar{Z}$ and $Z\bar{I}$ noises. It shows clearly in the figure that the fidelity is even further improved on top of the already-existing improvement from random twirling gates, which demonstrates that gate-level robustness from quantum control techniques can complement circuit compiling level robustness. As seen in Fig. 3(b), incorporating robust control pulses clearly im-

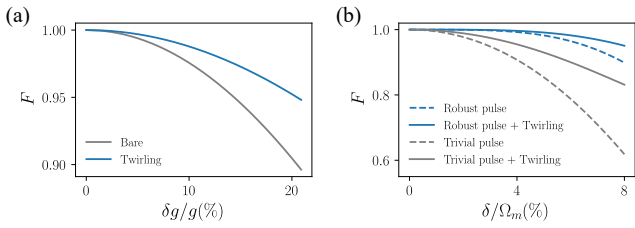


FIG. 3. State transfer fidelity of one single layer in the circuit of (a) iSWAP and (b) CNOT that transfer $|01\rangle$ to $|10\rangle$ and $1/\sqrt{2}(|0\rangle + |1\rangle)|0\rangle$ to $1/\sqrt{2}(|00\rangle + |11\rangle)$, respectively. The x-axis are the noise strength. Bare circuit and randomized compiled circuit are compared, and circuit with gates implemented with robust control pulse waveform (shown in Fig. 4) is also compared for CNOT circuit.

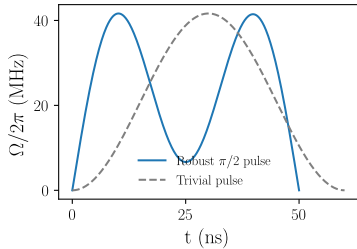


FIG. 4. The dephasing-robust optimized control pulse (blue) and the trivial cosine pulse (grey) for a $XX(\frac{\pi}{2})$ gate.

proves the fidelity, and the advantage gained from robust control is separated with RC.

We also visualized the noise channel to further analyze the effect of RC and robust control. The noise channel can be represented as a Pauli transfer matrix (PTM). The two figures on the left of Fig. 5 are the circuit without twirling gates, and the two on the right are the result when RC is used. We also incorporated robust quantum control techniques in the two figures at the bottom. Since RC could eliminate all cross terms in the noise channel and convert it into a Pauli channel, the corresponding PTM is a diagonal matrix where all the diagonal elements are given by Eq. 7. It also shows that the circuits implemented with robust control pulses have diagonal elements in the PTM of the noise channel more toward 1, indicating the fidelity enhancement by the robust control pulses.

In conclusion, we have extended the geometric framework from quantum dynamics to the circuit level, where the error accumulation from noise maps to a trajectory in the error geometric space. This trajectory's length signifies the error magnitude. By incorporating random twirling gates, what was once a deterministic trajectory is reshaped into a random walk process, substantially diminishing the worst-case error. Additionally, by averaging multiple equivalent circuits, we can eradicate noise coherence in the channel, transforming it into a Pauli

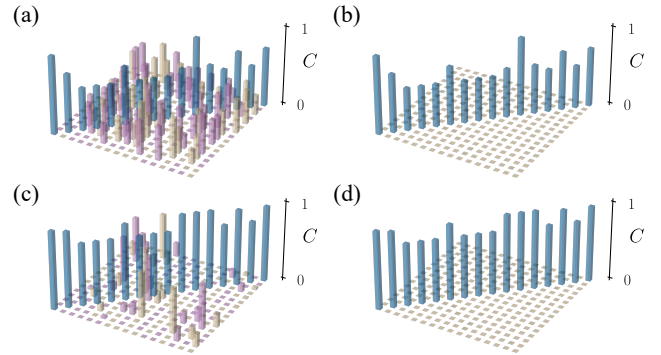


FIG. 5. PTM of the noise channel in the CNOT circuit under different conditions, where the diagonal elements are marked in blue; negative and non-negative off-diagonal elements are marked in plum and wheat, respectively. (a) Bare circuit with the trivial pulse, (b) Circuit with randomized compiling and trivial pulse, (c) Bare circuit with a robust pulse, and (d) Circuit with both randomized compiling and a robust pulse. The figures highlight how randomized compiling eliminates off-diagonal PTM terms, and robust pulses enhance the values of diagonal elements towards unity.

noise channel. The parameters of the noise channel can be extracted from the error distance of an individual quantum gate, also portrayed using the geometric formalism. We numerically demonstrate that incorporating robust quantum control techniques can further augment the circuit fidelity through various circuit examples. Looking forward, the quantum compiling process may be further optimized from this geometric perspective, potentially exceeding the improvements yielded by randomized compiling.

This work was supported by the Key-Area Research and Development Program of Guang-Dong Province (Grant No. 2018B030326001), the National Natural Science Foundation of China (U1801661), the Guangdong Innovative and Entrepreneurial Research Team Program (2016ZT06D348), the Guangdong Provincial Key Laboratory (Grant No.2019B121203002), the Natural Science Foundation of Guangdong Province (2017B030308003), and the Science, Technology and Innovation Commission of Shenzhen Municipality (JCYJ20170412152620376, KYTDPT20181011104202253), and the NSF of Beijing (Grants No. Z190012), Shenzhen Science and Technology Program (KQTD20200820113010023).

* dengxh@sustech.edu.cn

- [1] F. Arute, K. Arya, R. Babbush, D. Bacon, J. C. Bardin, R. Barends, R. Biswas, S. Boixo, F. G. Brandao, D. A. Buell, *et al.*, *Nature* **574**, 505 (2019).
- [2] Y. Wu, W.-S. Bao, S. Cao, F. Chen, M.-C. Chen, X. Chen, T.-H. Chung, H. Deng, Y. Du, D. Fan, *et al.*, *Phys. Rev. Lett.* **127**, 180501 (2021).

[3] A. J. Daley, I. Bloch, C. Kokail, S. Flannigan, N. Pearson, M. Troyer, and P. Zoller, *Nature* **607**, 667 (2022).

[4] C. D. B. Bentley, H. Ball, M. J. Biercuk, A. R. R. Carvalho, M. R. Hush, and H. J. Slatyer, arXiv:2005.00366 (2020), 2005.00366.

[5] N. Cody Jones, T. D. Ladd, and B. H. Fong, *New J. Phys.* **14**, 093045 (2012).

[6] C. L. Edmunds, C. Hempel, R. J. Harris, V. Frey, T. M. Stace, and M. J. Biercuk, *Phys. Rev. Research* **2**, 013156 (2020).

[7] T. J. Green, J. Sastrawan, H. Uys, and M. J. Biercuk, *New J. Phys.* **15**, 095004 (2013).

[8] I. Hansen, A. E. Seedhouse, A. Saraiva, A. Laucht, A. S. Dzurak, and C. H. Yang, *Phys. Rev. A* **104**, 062415 (2021).

[9] C. Kabytayev, T. J. Green, K. Khodjasteh, M. J. Biercuk, L. Viola, and K. R. Brown, *Phys. Rev. A* **90**, 012316 (2014).

[10] K. Khodjasteh, J. Sastrawan, D. Hayes, T. J. Green, M. J. Biercuk, and L. Viola, *Nat Commun* **4**, 2045 (2013).

[11] K. Khodjasteh, D. A. Lidar, and L. Viola, *Phys. Rev. Lett.* **104**, 090501 (2010).

[12] K. Khodjasteh and L. Viola, *Phys. Rev. Lett.* **102**, 080501 (2009).

[13] K. Khodjasteh and D. A. Lidar, *Phys. Rev. Lett.* **95**, 180501 (2005).

[14] F. Sauvage and F. Mintert, *Phys. Rev. Lett.* **129**, 050507 (2022).

[15] M. Veldhorst, C. Yang, J. Hwang, W. Huang, J. Dehollaïn, J. Muhonen, S. Simmons, A. Laucht, F. Hudson, K. M. Itoh, *et al.*, *Nature* **526**, 410 (2015).

[16] X. Xue, M. Russ, N. Samkharadze, B. Undseth, A. Sammak, G. Scappucci, and L. M. Vandersypen, *Nature* **601**, 343 (2022).

[17] A. R. Mills, C. R. Guinn, M. J. Gullans, A. J. Sigillito, M. M. Feldman, E. Nielsen, and J. R. Petta, *Science Advances* **8**, eabn5130 (2022).

[18] S. Sheldon, E. Magesan, J. M. Chow, and J. M. Gambetta, *Phys. Rev. A* **93**, 060302 (2016).

[19] P. Krantz, M. Kjaergaard, F. Yan, T. P. Orlando, S. Gustavsson, and W. D. Oliver, *Applied physics reviews* **6**, 021318 (2019).

[20] L. Egan, D. M. Debroy, C. Noel, A. Risinger, D. Zhu, D. Biswas, M. Newman, M. Li, K. R. Brown, M. Cetina, *et al.*, *Nature* **598**, 281 (2021).

[21] I. Pogorelov, T. Feldker, C. D. Marciniak, L. Postler, G. Jacob, O. Kriegelsteiner, V. Podlesnic, M. Meth, V. Negnevitsky, M. Stadler, *et al.*, *PRX Quantum* **2**, 020343 (2021).

[22] M. Werninghaus, D. J. Egger, F. Roy, S. Machnes, F. K. Wilhelm, and S. Filipp, *npj Quantum Information* **7**, 14 (2021).

[23] J. J. Wallman and J. Emerson, *Phys. Rev. A* **94**, 052325 (2016).

[24] A. Hashim, R. K. Naik, A. Morvan, J.-L. Ville, B. Mitchell, J. M. Kreikebaum, M. Davis, E. Smith, C. Iancu, K. P. O'Brien, I. Hincks, J. J. Wallman, J. Emerson, and I. Siddiqi, *Phys. Rev. X* **11**, 041039 (2021).

[25] Y. Gu, Y. Ma, N. Forcellini, and D. E. Liu, arXiv:2208.04100 (2022), arxiv:2208.04100.

[26] M. Urbanek, B. Nachman, V. R. Pascuzzi, A. He, C. W. Bauer, and W. A. de Jong, *Phys. Rev. Lett.* **127**, 270502 (2021).

[27] J. Zeng, X.-H. Deng, A. Russo, and E. Barnes, *New J. Phys.* **20**, 033011 (2018).

[28] J. Zeng and E. Barnes, *Phys. Rev. A* **98**, 012301 (2018).

[29] F. Zhuang, J. Zeng, S. E. Economou, and E. Barnes, *Quantum* **6**, 639 (2022).

[30] W. Dong, F. Zhuang, S. E. Economou, and E. Barnes, *PRX Quantum* **2**, 030333 (2021).

[31] D. Buterakos, S. Das Sarma, and E. Barnes, *PRX Quantum* **2**, 010341 (2021).

[32] Y.-J. Hai, J. Li, J. Zeng, D. Yu, and X.-H. Deng, arXiv:2210.14521 (2022).

[33] E. Barnes, F. A. Calderon-Vargas, W. Dong, B. Li, J. Zeng, and F. Zhuang, *Quantum Sci. Technol.* **7**, 023001 (2022).

[34] S. Roncallo, L. Maccone, and C. Macchiavello, *Phys. Rev. A* **107**, 022419 (2023).

[35] S. Chen, Y. Liu, M. Otten, A. Seif, B. Fefferman, and L. Jiang, *Nat Commun* **14**, 52 (2023).

[36] Z. Cai and S. C. Benjamin, *Scientific reports* **9**, 1 (2019).